

YIELDING CHARACTERISTIC AND NON-COAXIALITY OF TOYOURA SAND ON p' -CONSTANT SHEAR STRESS PLANE

HIROSHI OHKAWAⁱ⁾, JIRO KUWANOⁱⁱ⁾, TAKAFUMI NAKADAⁱⁱⁱ⁾ and SHINYA TACHIBANA^{iv)}

ABSTRACT

In order to investigate the deformation characteristics under a wide selection of stress history, ten series of stress probing tests on p' -constant shear stress plane on dense Toyoura sand are conducted by using hollow cylinder apparatus. This paper presents yielding behavior and non-coaxiality of Toyoura sand obtained from the tests. The stress probing tests consist of ten series of shearing tests each of which starts from systematically chosen individual initial stress point. Each initial stress point is subjected to load-unload stress history. The yielding characteristic is interpreted by means of a concept of multiple yield surfaces model which has three yield surfaces representing linearly elastic behavior limit, commencement point of rapid development in plastic strain and elasto-plastic range. As a result, an experimental evidence of the isotropic hardening, i.e., isotropic expansion of yield surface, induced by anisotropic loadings is obtained. This is what was tacitly assumed in the application of plastic flow rules. However, misalignment of directions between principal stress and principal plastic strain increment is observed. Moreover, plastic strain increment direction is found to be influenced by the given stress increment direction. These facts suggest the non-coaxiality between stress and plastic strain increment due to shear stress increment, even during monotonic loading with isotropic hardening. The plastic strain increment direction diverges from the normal direction to a surface which is a circle with its center nearly at the origin on p' -constant plane and which passes through the current stress point.

Key words: anisotropy, (elastic modulus), (isotropic hardening), laboratory test, (non-coaxiality), plasticity, sand, stress history, torsional shear, yield (IGC: D6)

INTRODUCTION

In recent years, constitutive models for predicting soil behavior have become more complex and included many parameters. Values of the parameters are generally obtained from in-situ or laboratory tests. Though the parameters should have physical meanings, some of these parameters are used for better fitting with individual experimental results. Therefore, it is important to accumulate data in various test conditions in establishing a constitutive model in general stress state.

There has been extensive research in the past on deformation characteristics of sand. Especially, yielding characteristic has been one of the main concerns. In conventional constitutive models for sand, generally, a point where maximum curvature appears on stress-strain relationship is often defined as a yield point. Then it is considered that deformation behavior is elastic under the yield point stress level and plastic over the yield point stress level. Studies on yielding of sand started from Poorooshasb et al. (1966, 1967), Scofield and Wroth

(1968) and Barden et al. (1969) in earnest. Subsequently, Nishi and Esashi (1978) and Vermeer (1978) proposed a model considering yielding behavior accompanied by consolidation, and then Tatsuoka and Molenkamp (1983) discussed about yield surface considering coupling effect of consolidation and shear deformation. The yielding characteristic at relatively low stress level was investigated by Ishihara and Okada (1978), Tanimoto and Tanaka (1986) and Tanimoto et al. (1987). Yielding characteristic at high stress level such as including particles crushing was studied by Miura and Yamamoto (1982) and Miura et al. (1984). The yielding characteristic from low stress level to high stress level was summarized and reported by Murata et al. (1987) and Yasufuku et al. (1991). In these models, deformation under the stress state within yield surface is usually assumed as linear elastic. Real soils, however, are highly non-linear and inelastic even within the yield surface. Therefore, deformation characteristics within the conventional yield surface are investigated in detail by Jardine (1992, 1995), Porovic (1995) and Zdravkovic and Jardine (1997). On the other hand, as a

ⁱ⁾ National Police Agency, Government of Japan, Tokyo, Japan (formerly Department of Civil Engineering, Tokyo Institute of Technology) (hookawa10@npa.go.jp).

ⁱⁱ⁾ Professor, Geosphere Research Institute, Saitama University, Saitama, Japan.

ⁱⁱⁱ⁾ Obayashi Corporation, Japan (formerly Department of Civil Engineering, Tokyo Institute of Technology).

^{iv)} Assistant Professor, Geosphere Research Institute, Saitama University, Saitama, Japan.

The manuscript for this paper was received for review on January 7, 2009; approved on October 1, 2010.

Written discussions on this paper should be submitted before September 1, 2011 to the Japanese Geotechnical Society, 4-38-2, Sengoku, Bunkyo-ku, Tokyo 112-0011, Japan. Upon request the closing date may be extended one month.

method to express complex behavior like kinematic hardening or hysteretic characteristics of continuous and composite systems, a concept of multiple yield surfaces was proposed by Mroz (1967) and Iwan (1967). The concept has been widely adopted to describe soil deformation characteristics and is called 'multiple yield surfaces model'. In this paper, the concept of multiple yield surfaces model which was interpreted by Jardine (1992) is adopted in discussing the test data.

The present study was carried out by using hollow cylinder apparatus, in which various stress states can be achieved, to investigate yielding characteristics of Toyoura sand. In many studies, the hollow cylinder apparatus has been used to conduct cyclic loading tests for investigating liquefaction or stiffness moduli. Some studies, however, have observed effects of principal stress rotation on deformation of sand (e.g., Ishihara and Towhata, 1983). Then, non-coaxiality or non-coincidence of principal stress and principal plastic strain increment directions have been recognized experimentally (e.g., Gutierrez and Ishihara, 2000).

The authors have investigated multiple yielding of Toyoura sand on p' -constant shear stress plane (Chaudhary and Kuwano, 2003; Kuwano et al., 2005; Kuwano and Nakada, 2005) as summarized by Ohkawa et al. (2008). In this paper, a new series of data on yielding characteristics and its anisotropy are presented, and non-coaxiality of stress and strain is discussed. In addition, quasi-elastic moduli at any stress states are also discussed briefly, as they are essential for evaluating plastic strain, which is important to discuss the yielding behavior and non-coaxiality.

TEST PROGRAM

A schematic diagram of the automated hollow cylinder apparatus used in this investigation is shown in Fig. 1. The specimen dimensions are height $h = 200$ mm, inner radius $r_i = 30$ mm and outer radius $r_o = 50$ mm. Details of the system development have been reported by

Nakamura et al. (1998), Chaudhary et al. (2004) and Ohkawa et al. (2008). All the measurement and control are made by PC through 16-bit A/D and D/A converters. The stress components of vertical stress σ_z , circumferential stress σ_θ , radial stress σ_r and torsional shear stress in z - θ plane $\tau_{z\theta}$ are applied to the specimen by controlling axial load W , torque M_T , inner cell pressure p_i and outer cell pressure p_o independently to each other as shown in Figs. 2 and 3. Axial load and cell pressures are controlled by air pressure through E/P transducers. Torque is controlled by a hydraulic pressure control unit. Axial load and torque are measured by internal load cells on the top cap of the specimen. The p_i and p_o are measured by pressure transducers at the base. Vertical strain ε_z and torsional shear strain in z - θ plane $\gamma_{z\theta}$ are measured by proximity transducers mounted on the top cap. Circumferential strain ε_θ and radial strain ε_r are calculated from the changes in the inner and outer radii of the specimen, r_i and r_o , obtained from the volume changes of the specimen and its hollow. The volume changes are measured by automated electronic balances whose accuracy is 0.001 g. The average stresses and corresponding strains are calculated as shown in Table 1. It should be noted that the stresses are not uniform across the wall of the hollow cylinder specimen in a general loading condition (e.g., Hight et al., 1983). The non-uniformity due to curvature for a given geometry of specimen and stress conditions is

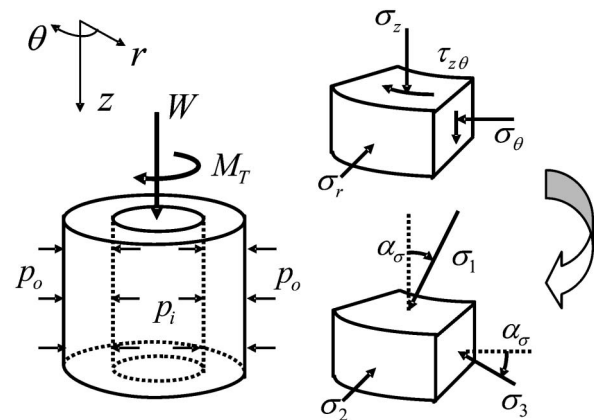


Fig. 2. External forces subjected to specimen and idealized stress condition in element

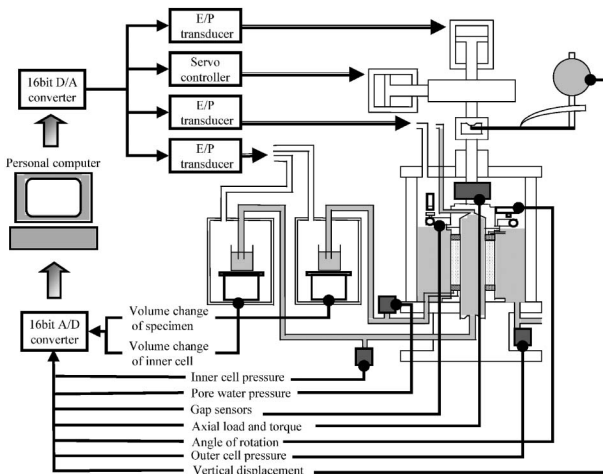


Fig. 1. Automated control system of hollow cylinder apparatus

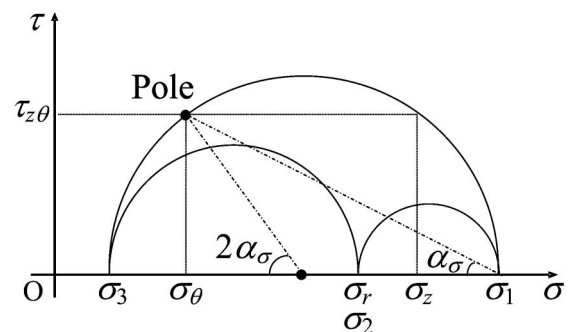


Fig. 3. Mohr stress circles of the stress condition in element

Table 1. Calculation of average stresses and strains in hollow cylinder specimen

Average stress	Average strain
$\sigma_z = \frac{W}{\pi(r_o^2 - r_i^2)} + \frac{p_o r_o^2 - p_i r_i^2}{r_o^2 - r_i^2} + \gamma' \frac{h}{2}$ $\sigma_r = \frac{r_o p_o + r_i p_i}{r_o + r_i} \quad \sigma_\theta = \frac{r_o p_o - r_i p_i}{r_o - r_i}$ $\tau_{z\theta} = \frac{1}{2} (\tau_{z\theta}^e + \tau_{z\theta}^p)$ <p>where</p> $\tau_{z\theta}^e = \frac{4M_T(r_o^3 - r_i^3)}{3\pi(r_o^4 - r_i^4)(r_o^2 - r_i^2)} \quad \tau_{z\theta}^p = \frac{3M_T}{2\pi(r_o^3 - r_i^3)}$	$\varepsilon_z = \frac{h}{h_i} = \frac{h_i - \Delta h}{h_i}$ $\varepsilon_r = -\frac{(r_o - r_{oi}) - (r_i - r_{ii})}{r_{oi} - r_{ii}} \quad \varepsilon_\theta = -\frac{(r_o - r_{oi}) + (r_i - r_{ii})}{r_{oi} + r_{ii}}$ $\gamma_{z\theta} = \frac{2\theta(r_{oi}^3 - r_{ii}^3)}{3h_i(r_o^2 - r_i^2)}$ <p>where</p> $r_i = \sqrt{\frac{1}{h} \left(r_{ii}^2 h_i - \frac{\Delta V_i}{\pi} \right)} \quad r_o = \sqrt{\frac{1}{h} \left(r_{oi}^2 h_i - \frac{\Delta V_i + \Delta V_s}{\pi} \right)}$
γ' : effective unit weight h : specimen height $\tau_{z\theta}^e$: $\tau_{z\theta}$ regarded as linear elastic body $\tau_{z\theta}^p$: $\tau_{z\theta}$ regarded as complete plastic body h_i : initial height of specimen Δh : vertical displacement of specimen	r_{ii} : initial inner radius of specimen r_{oi} : initial outer radius of specimen θ : torsional angle ΔV_i : volume change in inner cell ΔV_s : volume change in specimen

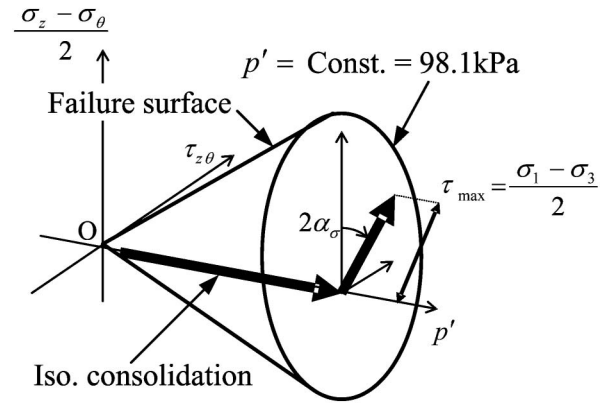
evaluated by assuming linear elasticity (Timoshenko and Goodier, 1970). As discussed by Gutierrez and Ishihara (2000), in which the specimen had the same inner and outer diameters as this study, the non-uniformity is sufficiently small for α_σ between 15° and 75° , where α_σ is the angle of major principal stress σ_1 from vertical direction (see Figs. 2, 3 and 4). The most serious non-uniformity appears in σ_θ at the inner wall for $\alpha_\sigma = 0^\circ$. For this reason, Pradel et al. (1990) suggested that average values of stresses and strains should be used to reduce the non-uniformity. The authors of this study accept their suggestions and also examined the accuracy of stress and strain measurements and the compliance corrections of the apparatus in detail. Values of small strain stiffness at the strain level of 0.001% obtained from this hollow cylinder apparatus are compatible to those obtained from the triaxial apparatus with bender elements (Chaudhary et al., 2004).

Toyoura sand specimens were reconstituted in the laboratory by air pluviation method with a relative density of approximately 80%. The index properties of Toyoura sand are summarized in Table 2. The specimens were saturated first by applying vacuum and then a back pressure of 196.2 kPa which was kept constant during shear. All the specimens were isotropically consolidated to mean effective pressure p' of 98.1 kPa and were allowed to creep for five or six hours so that the specimens were stabilized. Then, the specimens were sheared under drained conditions keeping p' constant as shown in Fig. 4. Coefficient of intermediate principal stress b was kept at 0.5 during shear. Therefore, $\sigma'_2 = \sigma'_r$ were kept constant as 98.1 kPa throughout the shearing process. Figure 5 shows the stress conditions during shear with $p' = \text{const.}$ and $b = \text{const.}$ in relation to Mohr (effective) stress circles.

The shearing tests consist of ten series. Shear stress paths on p' -constant plane are summarized in Fig. 6(a) for Series 1 to 6 and in Fig. 6(b) for Series 7 to 10. In Series 1, nine specimens were sheared along the stress paths to various α_σ directions from the isotropic stress

Table 2. Index properties of Toyoura sand

Specific gravity, G_s	2.645
Maximum void ratio, e_{\max}	0.973
Minimum void ratio, e_{\min}	0.609
Mean grain size, D_{50} (mm)	0.19
Effective grain size, D_{10} (mm)	0.14
Uniformity coefficient, U_c	1.56

**Fig. 4.** Illustration of isotropic consolidation and shearing on p' -constant plane

state point. A series of radial shearing tests to study the yielding behavior around any stress point is called hereafter as the “stress probing test”. In Series 2, six specimens were pre-sheared along $\alpha_\sigma = 22.5^\circ$ to $\tau_{\max} = (\sigma_1 - \sigma_3)/2 = 30$ kPa which is within Y_3 yield surface (defined later) obtained from Series 1, where σ_1 and σ_3 are the major and minor principal stresses respectively. Then, stress probing tests were carried out along six directions of $\alpha_{d\sigma}$. Here, it should be noted that $\alpha_{d\sigma}$ is the stress increment direction from the current stress point. In Series 3,

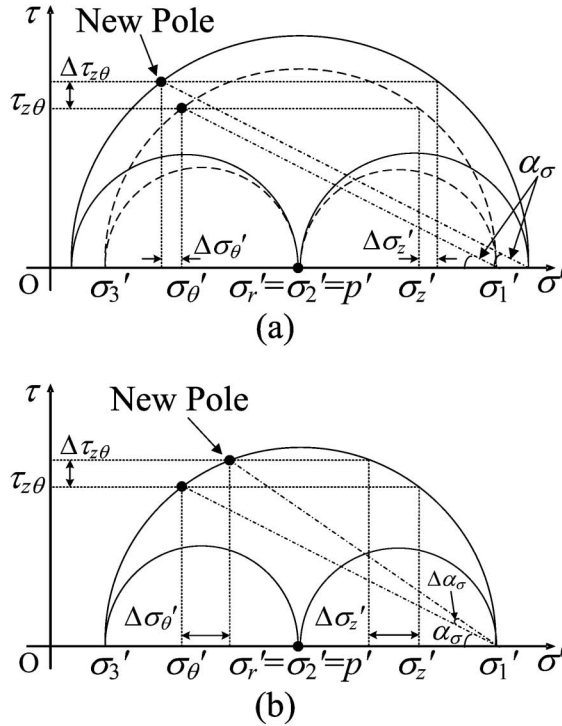


Fig. 5. Mohr (effective) stress circles during shear tests: (a) shearing at $\alpha_\sigma = \text{const.}$, $b = 0.5$ and $p' = \text{const.}$, and (b) shearing at $\tau_{\max} = \text{const.}$, $b = 0.5$ and $p' = \text{const.}$

six specimens were pre-sheared along $\alpha_\sigma = 67.5^\circ$ to $\tau_{\max} = 20$ kPa, then the stress probing tests were carried out. In Series 4 and 5, six specimens were pre-sheared along $\alpha_\sigma = 22.5^\circ$ to $\tau_{\max} = 39$ kPa and $\alpha_\sigma = 67.5^\circ$ to $\tau_{\max} = 30$ kPa respectively. Then the stress probing tests were carried out. In Series 6, four specimens were pre-sheared along $\alpha_\sigma = 45.0^\circ$ to $\tau_{\max} = 34$ kPa, then the stress probing tests were carried out. The initial points for stress probing tests in Series 4 to 6 are outside Y_3 yield surface obtained from Series 1. In Series 7, six specimens were pre-sheared along $\alpha_\sigma = 22.5^\circ$ to $\tau_{\max} = 39$ kPa which is outside the initial Y_3 surface, then unloaded to $\tau_{\max} = 30$ kPa along the same stress direction, and then the stress probing tests were carried out. In Series 8, six specimens were pre-sheared along $\alpha_\sigma = 67.5^\circ$ to $\tau_{\max} = 30$ kPa, then unloaded to $\tau_{\max} = 20$ kPa along the same stress direction, and then the stress probing tests were carried out. In Series 9, four specimens were pre-sheared along $\alpha_\sigma = 45.0^\circ$ to $\tau_{\max} = 34$ kPa, then unloaded to $\tau_{\max} = 27$ kPa along the same stress direction, and then the stress probing tests were carried out. In Series 10, six specimens were pre-sheared along $\alpha_\sigma = 0.0^\circ$ to $\tau_{\max} = 21$ kPa, then along $\alpha_{d\sigma} = 45.0^\circ$ to $\tau_{\max} = 30$ kPa, and then stress the probing tests were carried out. The initial points for the stress probing tests of Series 7 and 10 correspond to Series 2 while that of Series 8 corresponds to Series 3. In all the shear tests, shearing was halted temporarily at various maximum shear stress τ_{\max} and stress condition was kept for a few hours to observe creep characteristic of the sand. Then, small cyclic loads with the amplitude of ± 2 kPa, ± 4 kPa and -6 kPa were applied in the respective directions of $\Delta\sigma'_z$, $\Delta\sigma'_\theta$ and $\Delta\tau_{z\theta}$ to meas-

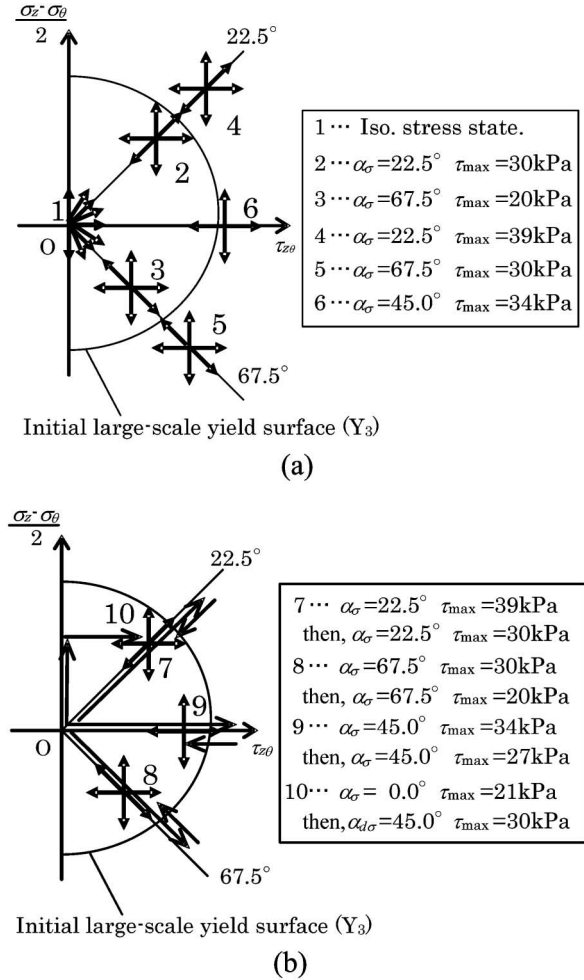


Fig. 6. Shearing stress paths for stress probing tests on p' -constant plane: (a) test series 1 to 6, and (b) test series 7 to 10

ure quasi-elastic moduli of E_z , E_θ and $G_{z\theta}$. The cyclic stress amplitude was changed to confirm linear elastic behavior in the stress-strain relationship. These creep and quasi-elastic moduli characteristics were mainly discussed by Nakamura et al. (1999), Kuwano et al. (1999) and Chaudhary et al. (2002, 2004). The quasi-elastic moduli characteristics are used to calculate elastic strain components for obtaining plastic strain components in this study. Therefore, the quasi-elastic modulus is further discussed in the following section.

ELASTIC MODULUS

It is widely appreciated that soil behavior is nonlinear except at very small strain level. Thus, evaluation of plastic strain becomes very important to discuss the soil behavior. In this study, the plastic strain was calculated by subtracting elastic strain component from total strain. Therefore, it is essential to evaluate elastic modulus accurately. It is well known that the elastic moduli have stress dependency, so called “quasi- (or pseudo-, or hypo-) elastic modulus”, and have cross-anisotropy when soils are deposited under gravity.

The small unload-reload cycles of $\Delta\sigma'_z$, $\Delta\sigma'_\theta$ and $\Delta\tau_{z\theta}$

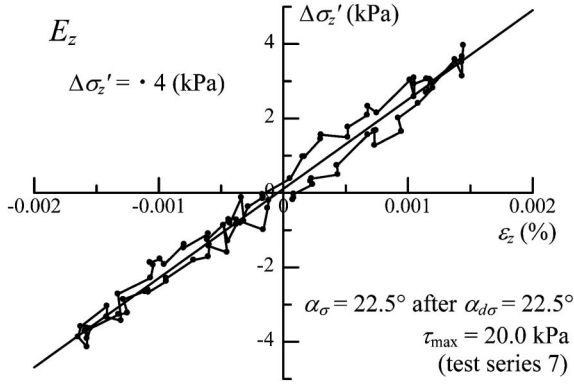


Fig. 7. Typical plots of stress-strain relationship obtained from small unload-reload cycles

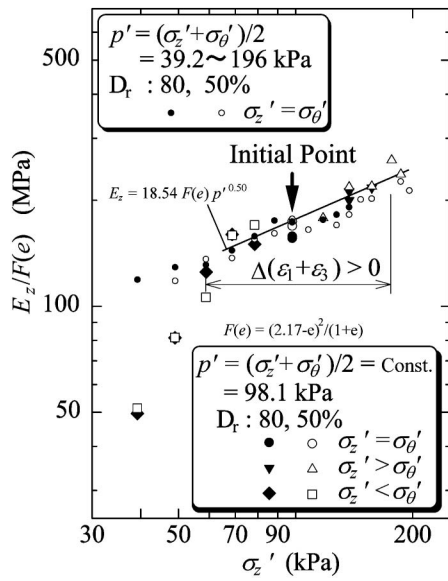


Fig. 8. Stress dependency of vertical Young's modulus E_z

during shear tests were applied to obtain elastic moduli, which are vertical and horizontal Young's moduli, E_z and E_θ , and torsional shear modulus $G_{z\theta}$, at various stress states. The moduli were determined by the slope of fitted straight line for stress-strain relationship (Fig. 7). The values of E_z are plotted against σ'_z in Fig. 8. E_z is divided by $F(e)$, shown later in Eq. (4), to take account of differences in void ratios among the specimens. Although Fig. 8 contains the data in different series of tests with $D_r = 50\%$, $E_z/F(e)$ of both densities follow the same straight line as shown in the figure. Therefore, small variations of density in this study can be removed properly. The data obtained in the isotropic stress state of $p' = 39.2 \sim 196$ kPa are also shown in the same figure to obtain the $E_z - \sigma'_z$ relationship for the isotropic stress condition.

The value of E_z for the isotropic stress condition is practically the same as E_z in anisotropic conditions ($\sigma'_z \neq \sigma'_\theta$) in the region of volume contraction, $\Delta(\varepsilon_1 + \varepsilon_3) > 0$, as seen in Fig. 8. However, in the dilatant region, $\Delta(\varepsilon_1 + \varepsilon_3) < 0$, E_z decreases rapidly with shear. Such a reduction in E_z after phase transformation was also shown by DEM

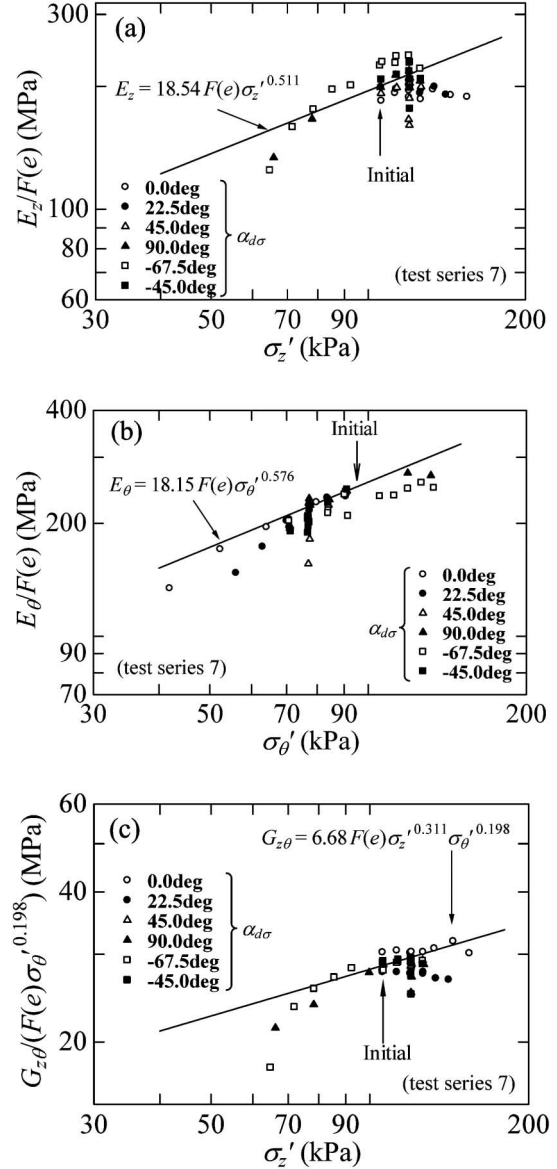


Fig. 9. Stress state dependency of the quasi-elastic moduli: (a) vertical Young's modulus E_z , (b) horizontal Young's modulus E_θ , and (c) torsional shear modulus $G_{z\theta}$

simulation (Ohba et al., 2001). Columns of particles are formed in the direction of compression with the increase in deviator stress. Although the ratio of contacts transmitting the normal force more than the double of the average, mostly in the direction of the columns, is almost constant after the phase transformation, the ratio of contacts which transmit less than half of the average force, mostly normal to the column, still increase gradually even after the phase transformation. It indicates that the lateral support of the column reduces and the columns become more fragile after the phase transformation. E_θ and $G_{z\theta}$ also show the same trend as E_z .

Typical results of the moduli obtained during shear test are shown in Fig. 9. The figure shows stress dependency of the moduli. Chaudhary et al. (2004) proposed equations for the moduli of Toyoura sand during isotropic consolidation ($p' = 20 \sim 200$ kPa) as follows:

$$\frac{E_z}{p_r} = 18.54F(e) \left(\frac{\sigma'_z}{p_r} \right)^{0.50} \quad (1)$$

$$\frac{E_\theta}{p_r} = 18.15F(e) \left(\frac{\sigma'_\theta}{p_r} \right)^{0.57} \quad (2)$$

$$\frac{G_{z\theta}}{p_r} = 6.68F(e) \left(\frac{\sigma'_z}{p_r} \right)^{0.35} \left(\frac{\sigma'_\theta}{p_r} \right)^{0.20} \quad (3)$$

where p_r is a reference pressure ($= 1.0$ kPa) and $F(e)$ is a function to remove scattering of void ratio, e , among test specimens (Hardin and Richart, 1963; Iwasaki et al., 1978), and given as:

$$F(e) = \frac{(2.17 - e)^2}{1 + e} \quad (4)$$

In Fig. 9, it is seen that data points around the initial state are on straight lines also for a series of shear tests. The straight lines can be expressed by adjusting slightly exponents of Eqs. (1) to (3).

$$\frac{E_z}{p_r} = 18.54F(e) \left(\frac{\sigma'_z}{p_r} \right)^{n_1} \quad (5)$$

$$\frac{E_\theta}{p_r} = 18.15F(e) \left(\frac{\sigma'_\theta}{p_r} \right)^{n_2} \quad (6)$$

$$\frac{G_{z\theta}}{p_r} = 6.68F(e) \left(\frac{\sigma'_z}{p_r} \right)^{n_3} \left(\frac{\sigma'_\theta}{p_r} \right)^{n_4} \quad (7)$$

The parameters n_1 , n_2 , n_3 and n_4 are determined by using all the data in radial shear tests as shown in Fig. 9.

The moduli show rapid decrease when shear stress level increases as discussed before. Thus, the decay of the moduli was estimated by the maximum shear strain γ_{\max} as shown in Fig. 10. It should be noted here that γ_{\max} is calculated considering the initial point for the stress probing test as the origin. Figure 10 shows the relationship between the moduli normalized by E_z^{cal} , E_θ^{cal} and $G_{z\theta}^{\text{cal}}$ obtained by the Eqs. (5) to (7) respectively and the maximum shear strain γ_{\max} . It can be said that Eqs. (5) to (7) are applicable for the strain level of 4×10^{-4} , and then the moduli decrease linearly with logarithm of γ_{\max} . Consequently, equations of the moduli can be rewritten as follows:

$$E_z = 18.54F(e)(\sigma'_z)^{n_1} f(\gamma_{\max}) \quad (8)$$

$$f(\gamma_{\max}) = 1 \quad (\gamma_{\max} \leq 0.0004)$$

$$f(\gamma_{\max}) = \alpha_1 - \beta_1 \log \gamma_{\max} \quad (\gamma_{\max} \geq 0.0004)$$

$$E_\theta = 18.15F(e)(\sigma'_\theta)^{n_2} f(\gamma_{\max}) \quad (9)$$

$$f(\gamma_{\max}) = 1 \quad (\gamma_{\max} \leq 0.0004)$$

$$f(\gamma_{\max}) = \alpha_2 - \beta_2 \log \gamma_{\max} \quad (\gamma_{\max} \geq 0.0004)$$

$$G_{z\theta} = 6.68F(e)(\sigma'_z)^{n_3} (\sigma'_\theta)^{n_4} f(\gamma_{\max}) \quad (10)$$

$$f(\gamma_{\max}) = 1 \quad (\gamma_{\max} \leq 0.0004)$$

$$f(\gamma_{\max}) = \alpha_3 - \beta_3 \log \gamma_{\max} \quad (\gamma_{\max} \geq 0.0004)$$

where α_1 , α_2 , α_3 , β_1 , β_2 and β_3 are determined by using test data as shown in Fig. 10. In this study, the plastic strain component was calculated using the equations for the quasi-elastic modulus mentioned above.

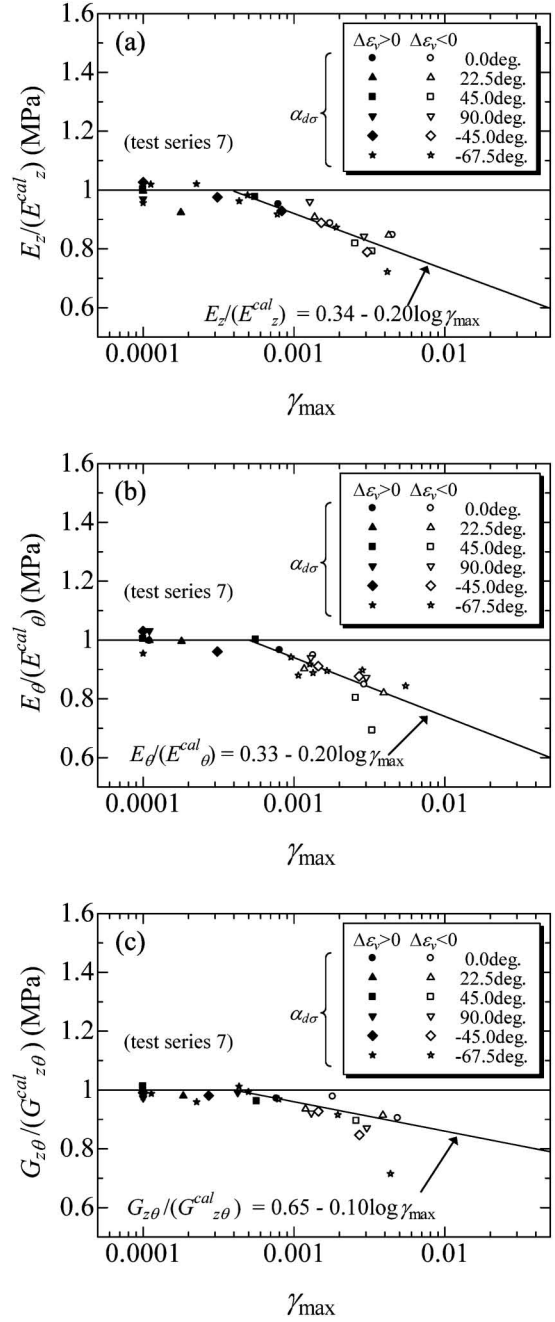


Fig. 10. Shear strain dependency of the quasi-elastic moduli: (a) vertical Young's modulus E_z , (b) horizontal Young's modulus E_θ , and (c) torsional shear modulus $G_{z\theta}$ (superscript cal means the value obtained from Eqs. (5), (6) and (7))

YIELDING CHARACTERISTICS

Determination of Yield Points

To describe the nonlinear behavior of soils within conventional yield surface, Jardine (1992) proposed multiple yield surfaces model shown in Fig. 11 where p' is effective confining pressure (or mean effective stress) and q is shear stress. It consists of three yield surfaces, Y_1 , Y_2 and Y_3 . The Y_3 yield surface represents large-scale yield surface, which is almost the same as conventional yield surface. The Y_1 surface represents the linear elastic limit and the Y_2 surface represents the recoverable range. The sub-yield

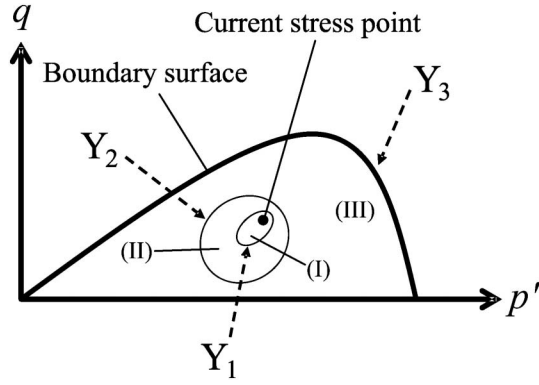


Fig. 11. Illustration of concept of multiple yield surfaces model interpreted by Jardine (1992): (I) linear elastic zone, (II) recoverable (i.e., nonlinear elastic) zone, and (III) plastic zone

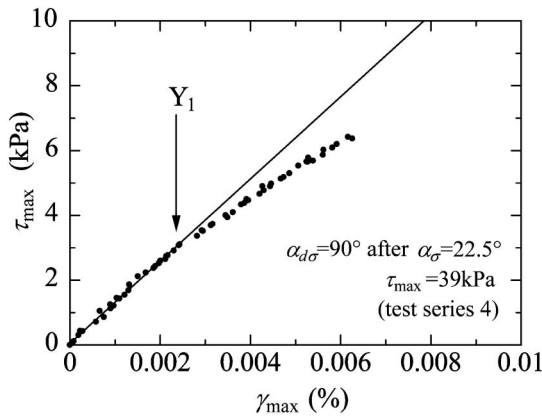


Fig. 12. Determination of Y_1 : linear elastic limit

surfaces Y_1 and Y_2 move with a current stress point. In this study, Jardine's model concept is applied to Toyoura sand and these three yield surfaces are identified in p' -constant shear plane and their characteristics are studied experimentally.

A typical relationship between maximum shear stress τ_{\max} and maximum shear strain γ_{\max} at small strain level is shown in Fig. 12. It can be observed that the relationship is linear up to a shear strain of approximately 0.002%. This point is designated as Y_1 . It should be noted here that τ_{\max} and γ_{\max} during a stress probing test are calculated considering the initial point for the stress probing test as the origin.

A typical relationship between the strain increment over 1 kPa of maximum shear stress τ_{\max} increment ($d\gamma_{\max}$) and γ_{\max} is given in Fig. 13. It can be seen that the $d\gamma_{\max}$ starts to develop rapidly at some point. This point is designated as Y_2 . Jardine (1992) defined Y_2 as the point where plastic strain increment starts to develop rapidly. Although we accept this definition in this study, slightly higher scatter was obtained at Y_2 strain level when we use plastic strain increment. Therefore, total strain increment is used in this study because the development of plastic strain increment results in development of total strain increment. Jardine et al. (1999) and Kuwano (1999) report-

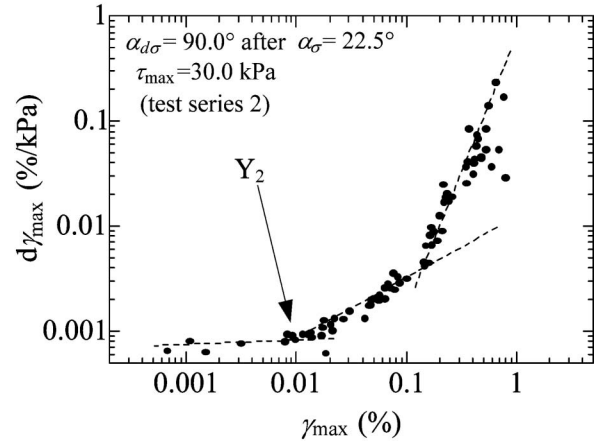


Fig. 13. Determination of Y_2 : start point of development in strain increment

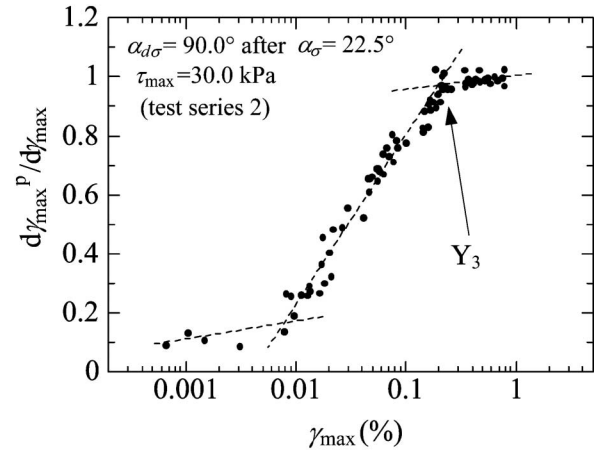


Fig. 14. Determination of Y_3 : almost complete plastic point

ed that Y_2 was also associated with a marked change in the direction of the plastic strain increment vector. Chaudhary and Kuwano (2003) reported shear modulus decreased rapidly around shear strain of Y_2 . Kuwano and Nakada (2005) showed plastic volumetric strain started to develop at the strain level of Y_2 . That is, Y_2 yield point represents rapid change in plastic characteristics of specimen. The range of shear strain at Y_2 yield point is between 0.005% and 0.01%.

A typical relationship between plastic strain increment ratio $d\gamma_{\max}^p/d\gamma_{\max}$ and γ_{\max} is given in Fig. 14. The plastic strain increment ratio $d\gamma_{\max}^p/d\gamma_{\max}$ represents the degree of plastic deformation. In Fig. 14, it can be observed that plastic strain increment ratio settled between 0.8 and 1.0. It represents that the sand completely yielded and strain increment became almost plastic in this strain level. This point is designated as Y_3 . It is obtained that the range of shear strain at Y_3 yield point is 0.05% to 0.15%.

Results and Discussion

Yield points explained above are plotted in p' -constant plane in Figs. 15(a) to (e). The yield characteristics are discussed based on these figures. The results from Series 1

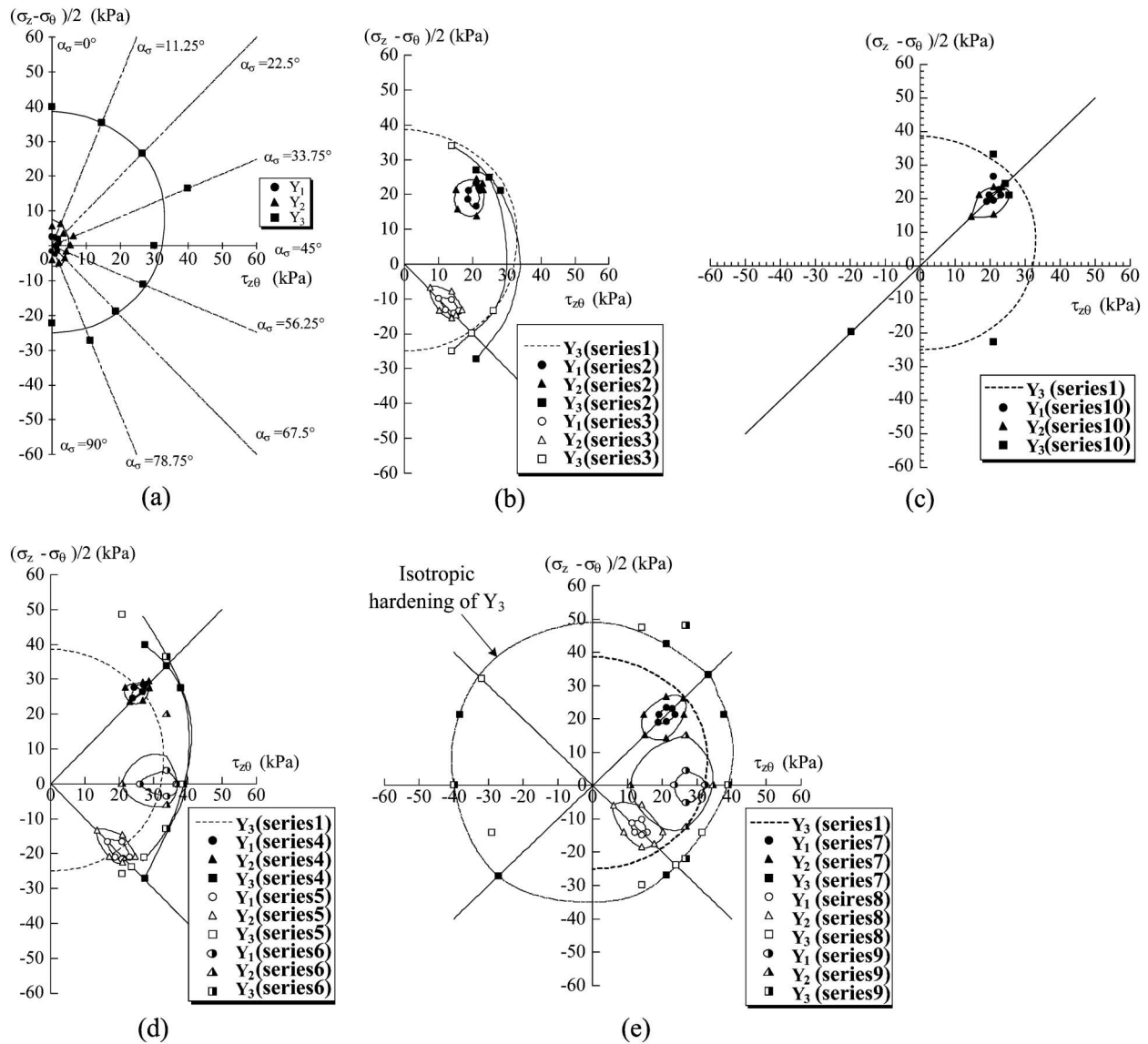


Fig. 15. Yielding characteristic: (a) test series 1, (b) test series 2 and 3, (c) test series 10, (d) test series 4, 5 and 6, and (e) test series 7, 8 and 9

are summarized in Fig. 15(a). In this series, tests were not carried out in area of $\tau_{z\theta} < 0$ because it can be considered that yielding characteristic is symmetrical with respect to $(\sigma_z - \sigma_\theta)/2$ axis. It is observed that Y_1 and Y_2 loci are roughly circular in shape and they are located at center of axes while Y_3 surface is almost a circle with its center shifted somewhat toward compression side, $(\sigma_z - \sigma_\theta)/2 > 0$. If a specimen is an isotropic material, the center of yield surface coincides with the origin of axes when the specimen was consolidated isotropically before shearing. Therefore, the specimen has inherent anisotropy as reported by many researchers (e.g., Arthur and Menzies, 1972). It is recognized that this anisotropy is caused by sedimentary structure formed under gravity. The result explains that inherent anisotropy of ground which is formed under gravity still exists after isotropic consolidation. Hence, it is necessary to consider that this anisotropy should be introduced to constitutive models as a parameter which explains degree of inherent

anisotropy. For example, assuming that Y_3 yield surface is a circle, its center is located at $(\sigma'_z - \sigma'_\theta)/2 \approx 7.5$ kPa and $\tau_{z\theta} = 0$ kPa from the test data. Thus, with the stress condition of $p' = 98.1$ kPa, we obtain $(\sigma'_z - \sigma'_\theta)/2p' \approx 0.076$. This value may be regarded as initial gradient of central axis of yield surface in p' - q stress plane at $p' = 98.1$ kPa.

The plots of yield loci obtained from Series 2 and 3 are given in Fig. 15(b). In these series, specimens were pre-sheared within initial Y_3 yield surface which are obtained from Series 1. The sub-yield loci Y_1 and Y_2 move with current stress point and they are now elliptical in shape, compared with circular in Series 1. They tend to orient along the direction of shearing. It is observed that Y_3 yield loci is approximately at the same place as that from Series 1, that is, Y_3 locus does not move with current stress point within initial Y_3 surface.

The results from Series 10, that the initial stress point for the stress probing tests is the same as that in Series 2 but with a different stress path to reach the stress point,

are shown in Fig. 15(c). Y_1 and Y_2 move with current stress point and are elliptical in shape similar to Series 2. However, observing the Y_1 and Y_2 in detail, it is seen that both Y_1 surface and Y_2 surface are oriented more to the direction of previous stress path (i.e., $\alpha_{ds} = 45.0^\circ$). This indicates that Y_1 and Y_2 yield surfaces were affected by previous stress path (Jardine et al., 1999). While, Y_3 yield surface locus is approximately at the same place as that from Series 1, 2 and 3 because current stress point is also still within initial Y_3 . This result indicates that Y_3 yield surface locus and shape are not affected by shear stress history within initial one.

The results from Series 4, 5 and 6 are shown in Fig. 15(d). The initial points for stress probing tests are outside of the initial Y_3 surface. The same tendency as Series 2 and 3 was obtained about Y_1 and Y_2 loci, moving with current stress point and being elliptical in shape oriented along the direction of shearing. On the other hand, Y_3 grows in size from the initial Y_3 surface. This indicates that the Y_3 surface is modified when it is intersected by the current stress point, and is not affected when the stress point is within the initial Y_3 surface. This is considered as hardening of the yield surface.

Shown in Fig. 15(e) are the results from Series 7, 8 and 9, in which the specimen was sheared to the outside of the initial Y_3 then unloaded to its inside. Like previous series, Y_1 and Y_2 move with current stress point and are elliptical in shape and orient along the direction of shearing. Regarding the size, however, different tendency is observed. Y_1 is almost the same in size as the other test series, while the size of Y_2 grows by load-unload shear stress history. In these test series, the shearing was made up to $\tau_{z\theta} < 0$ region and Y_3 yield surface can be drawn as a closed curve. As seen in Fig. 15(e), a single Y_3 yield surface is drawn for all the series of 7 to 9. The Y_3 surface is not affected by stress history. Y_3 locus is symmetric with respect to $(\sigma_z - \sigma_\theta)/2$ axis. The size of Y_3 is approximately the same as expanded Y_3 surface obtained in Series 4, 5 and 6. This indicates that Y_3 yield surface shows isotropic hardening by loading, with the shape being kept almost circular, and its center is slightly shifted upward at $(\sigma'_z - \sigma'_\theta)/2 \approx 10.0$ kPa and $\tau_{z\theta} = 0$ kPa. Therefore, in the same way as Series 1, we obtain $(\sigma'_z - \sigma'_\theta)/2p' \approx 0.102$ in this case. It indicates the slight shifting of the center of Y_3 , or rotation of the axis of Y_3 center in the stress space as shown in Fig. 4.

NON-COAXIALITY

Previous Studies

It is well known that non-coincidence of principal stress and principal plastic strain increment directions, so-called “non-coaxiality”, often appears in granular materials. It is considered that the non-coaxiality is caused by stress history, anisotropy of materials, or stress increment direction. Experimental evidence for non-coaxiality is based on the micro-mechanical study of Drescher and de Josselin de Jong (1972) using a photo-elastic disc assembly as a two-dimensional analog of

granular media. Attempts have been made to describe the non-coaxial behavior of granular materials by using double sliding model (e.g., de Josselin de Jong, 1988). On the other hand, there is another field where non-coaxiality has been focused on. The focus is a role of non-coaxiality in formation of shear band and a need to introduce a non-coaxiality flow rule to constitutive models in order to obtain a better estimate of the onset of strain localization (e.g., Hill and Hutchinson, 1975; Rundnicki and Rice, 1975). These previous studies on non-coaxiality were summarized by Gutierrez and Ishihara (2000) in detail.

Plastic Strain Increment

Figure 16 represents plastic strain increment directions on initial Y_3 surface which was obtained from Series 1. In this figure, solid arrows indicate the plastic strain increments which are experimentally obtained by the Series 2 and 3, and chained-long arrows show shear stress paths. Each plastic strain increment is calculated by subtracting elastic strain increment from total strain increment using the quasi-elastic moduli estimated in previous chapter. Superscript p in Fig. 16 means plastic component of strains. While, dotted arrows are normal to Y_3 surface which is regarded as a shape of circle. Plastic strain increment arrows do not mean vector, but, illustrate only direction. It seems that plastic strain increment directions obtained by experiments are almost normal to Y_3 surface. However, in more detailed observation, it can be seen that plastic strain increment directions incline to the applied stress path and this tendency appears more clearly in case that the stress path has a wider angle from the normal to Y_3 surface. Therefore, these experimental results suggest the existence of non-coaxiality of Toyoura sand due to applied shear stress increment during monotonic loading.

There have been proposed several elasto-plastic non-coaxial constitutive models in which the plastic (or inelastic) strain increment (rate) is predicted by not only ap-

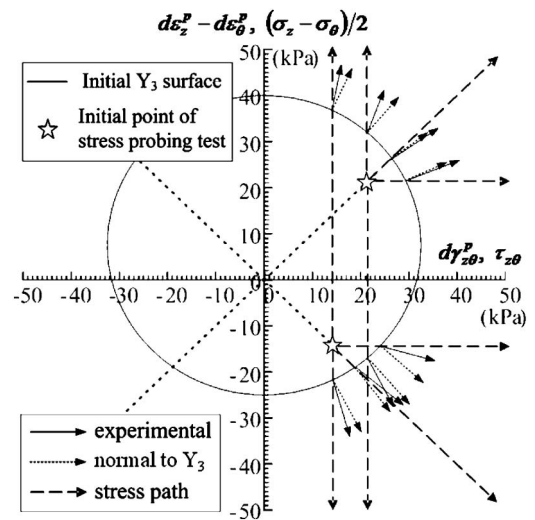


Fig. 16. Plastic strain increment directions on initial Y_3 surface on p' -constant plane

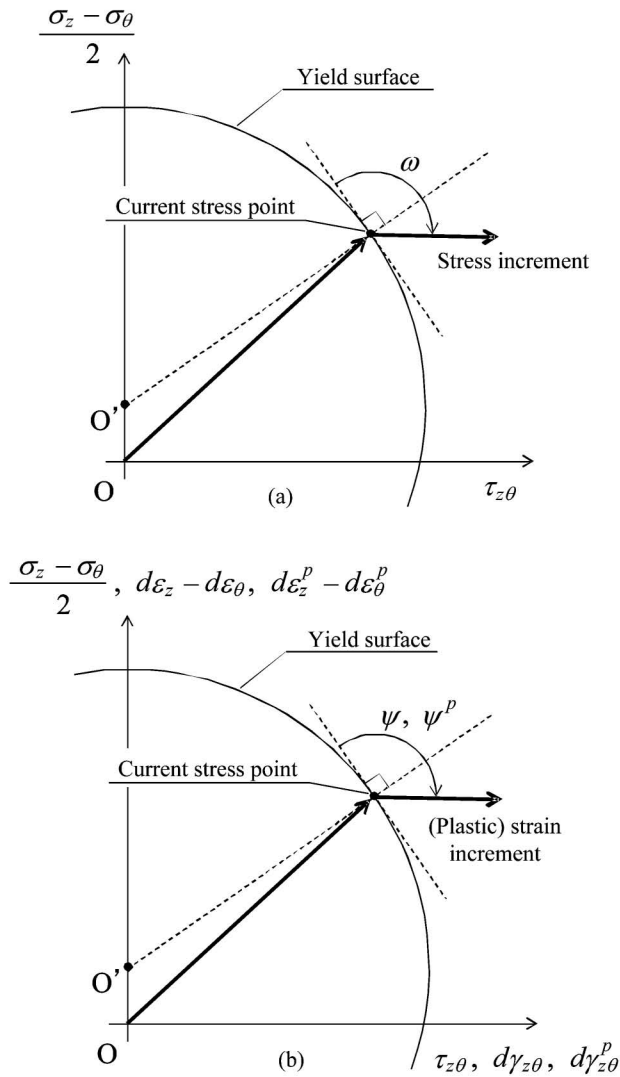


Fig. 17. Definition of stress and (plastic) strain increment angles on p' -constant plane: (a) stress increment, and (b) plastic and total strain increment

plying associated flow rule but introducing stress increment (rate) effects (e.g., Yatomi et al., 1989; Hashiguchi and Tsutsumi, 2003). Taking their concepts into account, then, we shall estimate and discuss the off-normal angles of plastic strain increment to yield surface.

As non-coaxiality appears clearly when principal stress rotation occurs, the initial points of stress probing tests should be focused on. Regarding the initial points of stress probing test as current stress points, the shear stress and (plastic) shear strain increment directions from current stress point are measured as shown in Fig. 17. In order to discuss the non-coaxiality which is induced only by stress increment direction, we assume the following to define a yield surface passing through the current stress and its characteristics: i) the yield surface is circular in shape and its center is located at $(\sigma'_z - \sigma'_\theta)/2 = 10.0$ kPa and $\tau_{z\theta} = 0$ kPa for all the test series, ii) the yield surface grows isotropically when the current stress point moves to outward the surface, and iii) the yield surface is fixed when the current stress point moves to unloading direc-

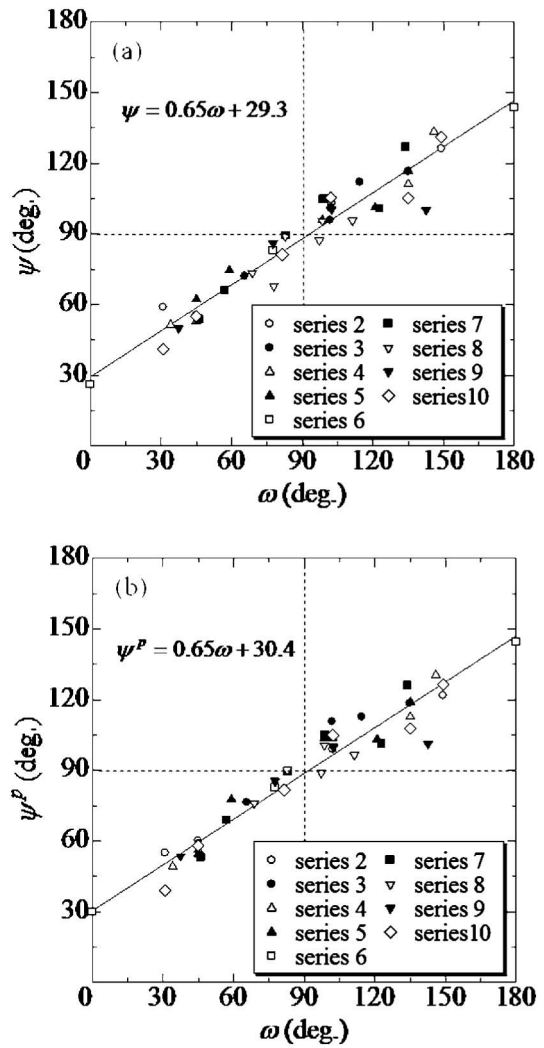


Fig. 18. Relationship between shear stress and shear strain increment angle on yield surface: (a) total shear strain increment angle, and (b) plastic shear strain increment angle

tion. These assumptions are based on the results of Y_3 yield surface characteristics shown in previous chapter.

Results and Discussion

Figure 18 shows relationship between shear stress increment direction ω and total or plastic shear strain increment direction ψ or ψ^p on the yield surface. The total shear strain increment has almost the same direction as the plastic strain increment, because stress states at which the angles are measured are relatively high and are relatively high plastic region. In unloading process (e.g., stress probing test toward inside of the current yield surface from the stress point A in Fig. 19), it can be considered that deformation behavior is elastic at early stage. Therefore, the angles were measured at points, i.e., B to D, where stress path reaches the same value of maximum shear stress τ_{\max} as point A. It could be confirmed only after the experiments that the yielding was achieved at that point. If associated flow rule is employed with the yield surface, the plastic strain increment angles have to become always 90° in Fig. 18(b). However, it can be seen

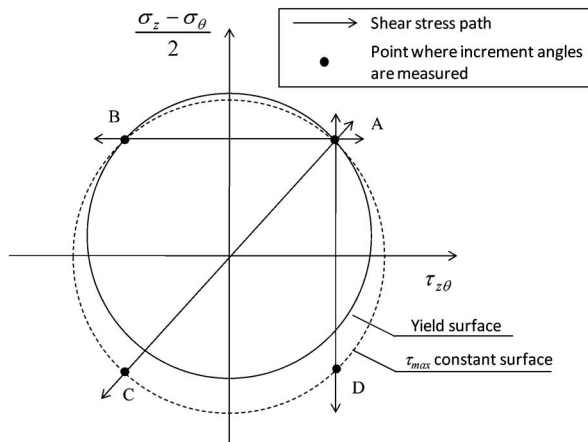


Fig. 19. Points where stress and (plastic) strain increment angles are measured

that the directions of total and plastic shear strain increment vary with changing in shear stress increment direction. When the stress increment angle ω is equal to 90° , the strain increment angle ψ or ψ^p is almost 90° . On the other hand, it can be observed that the shear strain increment direction obviously inclines to the shear stress increment direction. Therefore, following the concept of Yatomi et al. (1989), and Hashiguchi and Tsutsumi (2003), it can be said that (plastic) strain increment direction is clearly influenced by stress increment direction. That is, non-coaxiality is induced by stress increment direction. Here, it is noted that ψ^p should be indefinite theoretically when ω is 0° or 180° , because $\omega = 0^\circ$ or 180° does not strictly mean plastic loading. However, a certain amount of plastic strain increment was observed in the shear toward the direction almost tangent to Y_3 . Strain increment direction in this shear is in consistent with others as seen in Fig. 18 and diverted to the direction normal to Y_3 . A degree of non-coaxiality should be discussed and compared with mathematical development as further study.

In this study, it is assumed that deformation behavior is elastic within the yield surface introduced in this chapter. However, elastic range is very small as shown in experimental results of Y_2 surface characteristics. As non-coaxial behavior relates to plastic strain, it can be considered that Y_2 yield surface which represents rapid development of plastic strain is a key to discuss non-coaxial behavior within the yield surface.

CONCLUSIONS

The yielding characteristics of dense Toyoura sand on p' -constant shear stress plane with $b=0.5$ were investigated by introducing two sub-yield surfaces Y_1 and Y_2 inside the large-scale yield surface Y_3 . They are almost circular in shape when shearing is carried out from the isotropic stress state. When the specimen is sheared from the isotropic stress state, the centers of Y_1 and Y_2 surfaces locate at the origin and the Y_3 surface center shifts towards compression side indicating anisotropic charac-

teristics of dense Toyoura sand. This inherent anisotropy of Y_3 surface can be regarded as the initial gradient of central axis of Y_3 yield surface in p' - q stress plane. On the other hand, anisotropy of Y_1 and Y_2 increased with the progress of shearing. The sub-yield surfaces move with the current stress state and become elliptical shape. They seem to tend to orient along the most recent stress path. After load-unload shear stress history, Y_2 surface becomes large. The large-scale yield surface Y_3 is comparatively immobile. It stays around the isotropic stress state point. However, it expands when it is intersected by the current stress point. It shows isotropic hardening and is also likely to show rotational hardening.

The plastic strain increment direction is not normal to the Y_3 yield surface and inclines to the stress increment direction. In order to find experimental evidence of non-coaxiality, test data was reappraised using the concept of non-coaxiality term caused by stress increment direction. It is seen that Toyoura sand has non-coaxiality of principal stress and principal plastic strain increment directions even during monotonic shearing with isotropic hardening.

ACKNOWLEDGEMENTS

A part of test data presented in this paper was obtained by Dr. Chaudhary, S. K. of Navajo Nation Environmental Protection Agency, USA, Mr. Hashimoto, S. of Asahi Kasei Homes, Mr. Ohba, H. of Railway Technical Research Institute (formerly Department of Civil Engineering, Tokyo Institute of Technology). The authors wish to express their gratitude for their achievements. The help and advice provided by Prof. Kusakabe, O. and Prof. Ohta, H. of Tokyo Institute of Technology and Prof. Iizuka, A. of Kobe University are greatly appreciated.

REFERENCES

- 1) Arthur, J. R. F. and Menzies, B. K. (1972): Inherent anisotropy in a sand, *Geotechnique*, **22**(1), 115-128.
- 2) Barden, L., Ismail, H. and Tong, P. (1969): Plane strain deformation of granular material at low and high pressures, *Geotechnique*, **19**(4), 441-452.
- 3) Chaudhary, S. K., Kuwano, J., Hashimoto, S., Hayano, Y. and Nakamura, Y. (2002): Effects of initial fabric and shearing direction on cyclic deformation characteristics of sand, *Soils and Foundations*, **42**(1), 147-157.
- 4) Chaudhary, S. K. and Kuwano, J. (2003): Anisotropic multiple yielding of dense Toyoura sand in p' -constant shear plane, *Soils and Foundations*, **43**(4), 59-69.
- 5) Chaudhary, S. K., Kuwano, J. and Hayano, Y. (2004): Measurement of quasi-elastic stiffness parameters of dense Toyoura sand in hollow cylinder apparatus and triaxial apparatus with bender elements, *Geotech. Testing J.*, GTJODJ, **27**(1), 23-35.
- 6) de Josselin de Jong, G. (1988): Elasto-plastic version of the double sliding model in undrained simple shear test, *Geotechnique*, **38**(4), 533-555.
- 7) Drescher, A. and de Josselin de Jong, G. (1972): Photoelastic verification of a mechanical model for the flow of a granular material, *J. Mech. Phys. Solids*, **20**(5), 337-351.
- 8) Gutierrez, M. and Ishihara, K. (2000): Non-coaxiality and energy

- dissipation in granular materials, *Soils and Foundations*, **40**(2), 49–59.
- 9) Hardin, B. O. and Richart, F. E., Jr. (1963): Elastic wave velocities in granular soils, *J. SMF Div.*, ASCE, **89**(1), 33–65.
 - 10) Hashiguchi, K. and Tsutsumi, S. (2003): Shear band formulation analysis in soils by the subloading surface model with tangential stress rate effect, *Int. J. Plasticity*, **19**(10), 1651–1677.
 - 11) Hight, D. W., Gens, A. and Symes, M. J. (1983): The development of a new hollow cylinder apparatus for investigating the effects of principal stress rotation in soils, *Geotechnique*, **33**(4), 355–383.
 - 12) Hill, R. and Hutchinson, J. W. (1975): Bifurcation phenomena in the plane tension test, *J. Mech. Phys. Solids*, **23**(4/5), 239–264.
 - 13) Ishihara, K. and Okada, S. (1978): Yielding of overconsolidated sand and liquefaction model under cyclic stresses, *Soils and Foundations*, **18**(1), 57–72.
 - 14) Ishihara, K. and Towhata, I. (1983): Sand response to cyclic rotation of principal stress directions as induced by wave loads, *Soils and Foundations*, **23**(4), 11–26.
 - 15) Iwan, W. D. (1967): On a class of models for the yielding behaviour of continuous and composite systems, *J. Appl. Mech.*, ASME, **34**(3), 612–617.
 - 16) Iwasaki, T., Tatsuoka, F. and Takagi, Y. (1978): Shear moduli of sands under cyclic torsional shear loading, *Soils and Foundations*, **18**(1), 39–56.
 - 17) Jardine, R. J. (1992): Some observations on the kinematic nature of soil stiffness, *Soils and Foundations*, **32**(2), 111–124.
 - 18) Jardine, R. J. (1995): Keynote Lecture: One perspective of the pre-failure deformation characteristics of some geomaterials, *Proc. Int. Symp. Pre-failure Deformation Characteristics of Geomaterials*, Sapporo, **2**, 855–885.
 - 19) Jardine, R. J., Kuwano, R., Zdravkovic, L. and Thornton, C. (1999): Theme and Keynote Lecture: Some fundamental aspects of the pre-failure behaviour of granular soils, *Proc. 2nd Int. Symp. Pre-failure Deformation Characteristics of Geomaterials*, Torino, **2**, 1077–1113.
 - 20) Kuwano, J., Nakamura, Y. and Hashimoto, S. (1999): Anisotropy of small-strain stiffness and creep of Toyoura sand under various stress conditions, *Proc. 11th ARCSMGE*, Seoul, **1**, 53–56.
 - 21) Kuwano, J. and Nakada, T. (2005): Effects of shear stress history on yielding of dense Toyoura sand in p' -constant shear plane, *Proc. 16th ICSMGE*, Osaka, **2**, 527–530.
 - 22) Kuwano, J., Chaudhary, K. and Ohba, H. (2005): Change in multiple yield surfaces of dense Toyoura sand with shearing in a p' -constant plane, *Geomechanics: Testing, Modeling, and Simulation*, Geotechnical Special Publication, (eds. by Yamamuro and Koseki), ASCE, **143**, 319–340.
 - 23) Kuwano, R. (1999): The stiffness and yielding anisotropy of sand, *Ph. D. Thesis*, Imperial College, University of London.
 - 24) Miura, N. and Yamamoto, N. (1982): On the yield curve of sand in a particle-crushing region, *Proc. JSCE*, **326**, 83–90 (in Japanese).
 - 25) Miura, N., Murata, H. and Yasufuku, N. (1984): Stress-strain characteristics of sand in a particle-crushing region, *Soils and Foundations*, **24**(1), 77–89.
 - 26) Mroz, Z. (1967): On the description of anisotropic work hardening, *J. Mech. Phys. Solids*, **15**(3), 163–175.
 - 27) Murata, H., Hyodo, M. and Yasufuku, N. (1987): Yield characteristics of dense sand under low and high pressure, *Proc. JSCE*, **382**, 183–192 (in Japanese).
 - 28) Nakamura, Y., Hashimoto, S. and Kuwano, J. (1998): The development of a hollow cylinder apparatus for a measurement in a wide strain range, *Proc. 33rd JNCGE*, Yamaguchi, JGS, **1**, 519–520 (in Japanese).
 - 29) Nakamura, Y., Kuwano, J. and Hashimoto, S. (1999): Small-strain stiffness and creep of Toyoura sand measured by a hollow cylinder apparatus, *Proc. 2nd Int. Symp. on Pre-failure Deformation Characteristics of Geomaterials*, **1**, 141–148.
 - 30) Nishi, K. and Esashi, Y. (1978): Stress-strain relationships of sand based on elasto-plasticity theory, *Proc. JSCE*, **280**, 111–122.
 - 31) Ohba, H., Chaudhary, S. K., Matsushima, T., Kuwano, J. and Takahashi, A. (2001): DEM simulation of anisotropic shear behavior of granular material, *Proc. 36th JNCGE*, Tokushima, **1**, 507–508 (in Japanese).
 - 32) Ohkawa, H., Kuwano, J., Kusakabe, O. and Ohta, H. (2008): Study on deformation characteristics of Toyoura sand by using hollow cylinder apparatus, *J. Appl. Mech.*, JSCE, **11**, 377–388 (in Japanese).
 - 33) Poorooshasb, H. B., Holubec, I. and Sherbourne, A. N. (1966): Yielding and flow of sand in triaxial compression, part I, *Can. Geotech. J.*, **3**(4), 179–190.
 - 34) Poorooshasb, H. B., Holubec, I. and Sherbourne, A. N. (1967): Yielding and flow of sand in triaxial compression, part II and III, *Can. Geotech. J.*, **4**(4), 376–397.
 - 35) Porovic, E. (1995): Investigations of soil behaviour using a resonant-column torsional-shear hollow cylinder apparatus, *Ph. D. Thesis*, Imperial College, University of London.
 - 36) Pradel, D., Ishihara, K. and Gutierrez, M. (1990): Yielding and flow of sand under principal stress axes rotation, *Soils and Foundations*, **30**(1), 87–99.
 - 37) Rudnicki, J. W. and Rice, J. R. (1975): Conditions for the localization of deformation in pressure-sensitive dilatant materials, *J. Mech. Phys. Solids*, **23**(6), 371–394.
 - 38) Schofield, A. and Wroth, P. (1968): *Critical State Soil Mechanics*, McGraw-Hill, London, 310.
 - 39) Tanimoto, K. and Tanaka, Y. (1986): Yielding of soil as determined by acoustic emission, *Soils and Foundations*, **26**(3), 69–80.
 - 40) Tanimoto, K., Tanaka, Y. and Kagotani, N. (1987): The effect of pre-shearing on yield locus of sandy soil, *Proc. 8th ARCSMFE*, Kyoto, **1**, 105–108.
 - 41) Tatsuoka, F. and Molenkamp, F. (1983): Discussion on yield loci for sands, *Mechanics of Granular Materials: New Models and Constitutive Relations*, (eds. by Jenkins, J. T. and Satake, M.), Elsevier Science Publishers B. V., 75–87.
 - 42) Timoshenko, S. P. and Goodier, J. N. (1970): *Theory of Elasticity* (1934). Third Edition, Kosaide Printing Co. Ltd., Tokyo, 567.
 - 43) Vermeer, P. A. (1978): A double hardening model for sand, *Geotechnique*, **28**(4), 413–433.
 - 44) Yasufuku, N., Murata, H. and Hyodo, M. (1991): Yield characteristics of anisotropically consolidated sand under low and high stresses, *Soils and Foundations*, **31**(1), 95–109.
 - 45) Yatomi, C., Yashima, A., Iizuka, A. and Sano, I. (1989): General theory of shear bands formation by a non-coaxial Cam-clay model, *Soils and Foundations*, **29**(3), 41–53.
 - 46) Zdravkovic, L. and Jardine, R. J. (1997): Some anisotropic stiffness characteristics of a silt under general stress conditions, *Geotechnique*, **47**(3), 407–437.